Acidities of confined water in interlayer space of clay minerals

Liu, X.; Lu, X.; Wang, R.; Meijer, E.J.; Zhou, H.

DOI
10.1016/j.gca.2011.06.011

Publication date
2011

Document Version
Final published version

Published in
Geochimica et Cosmochimica Acta

Available online at www.sciencedirect.com
ScienceDirect
Geochimica et Cosmochimica Acta 75 (2011) 4978–4986
Geochimica et Cosmochimica Acta
www.elsevier.com/locate/gca

Acidities of confined water in interlayer space of clay minerals

Xiandong Liu [a,*], Xiancai Lu [a], Rucheng Wang [a], Evert Jan Meijer [b], Huiqun Zhou [a]

[a] State Key Laboratory for Mineral Deposits Research, School of Earth Sciences and Engineering, Nanjing University, Nanjing 210093, PR China
[b] Van't Hoff Institute for Molecular Sciences and Amsterdam Center for Multiscale Modeling, University of Amsterdam, Nieuwe Achtergracht 166, 1018 WV Amsterdam, The Netherlands

Received 6 December 2010; accepted in revised form 8 June 2011; available online 15 June 2011

Abstract

The acid chemistry of confined waters in smectite interlayers have been investigated with first principles molecular dynamics (FPMD) simulations. Aiming at a systematic picture, we establish the model systems to take account of the three possible controlling factors: layer charge densities (0 *e*, 0.5 *e* and 1.0 *e* per cell), layer charge locations (tetrahedral and octahedral) and interlayer counterions (Na^+ and Mg^{2+}). For all models, the interlayer structures are characterized in detail. Na^+ and Mg^{2+} show significantly different hydration characteristics: Mg^{2+} forms a rigid octahedral hydration shell and resides around the midplane, whereas Na^+ binds to a basal oxygen atom and forms a very flexible hydration shell, which consists of five waters on average and shows very fast water exchanges. The method of constraint is employed to enforce the water dissociation reactions and the thermodynamic integration approach is used to derive the free-energy values and the acidity constants. Based on the simulations, the following points have been gained. (1) The layer charge is found to be the direct origin of water acidity enhancement in smectites because the neutral pore almost does not have influences on water dissociations but all charged pores do. (2) With a moderate charge density of 0.5 *e* per cell, the interlayer water shows a p*K*a value around 11.5. While increasing layer charge density to 1.0 *e*, no obvious difference is found for the free water molecules. Since 1.0 *e* is at the upper limit of smectites' layer charge, it is proposed that the calculated acidity of free water in octahedrally substituted Mg^{2+}-smectite, 11.3, can be taken as the lower limit of acidities of free waters. (3) In octahedrally and tetrahedrally substituted models, the bound waters of Mg^{2+} show very low p*K*a values: 10.1 vs 10.4. This evidences that smectites can also promote the dissociations of the coordinated waters of metal cations. The comparison between the two Mg^{2+}-smectites reveals that different layer charge locations do not lead to obvious differences for bound and free water acidities.

1. INTRODUCTION

Confined waters are ubiquitous in nature and they play important roles in geological, biological and technical processes (Wang et al., 2003; Brovchenko and Oleinikova, 2008). Water under confinement shows different behaviors from the bulk due to the influences from the limiting boundaries and this has received great attention (Dysthe and Wogelius, 2006; Brovchenko and Oleinikova, 2008). Smectites, a big family of 2:1 type phyllosilicates, widely distribute in soils and sediments and they contain considerable confined waters in their interlayer pores (Grim, 1962; Bergaya et al., 2006). The layering structure of smectites is formed by stacking along *c*-axis the "T–O–T" layers, which consist of an octahedral sheet sandwiched by two tetrahedral sheets (Grim, 1962; Brindley and Brown, 1980; Bleam, 1993). Therefore, 2-D pores are made by the opposite "T–O–T" layers. The isomorphic substitutions in octahedral and/or tetrahedral sheets make the clay frameworks bear negative charges, which are compensated by interlayer counterions. Water and organics can enter interlayer regions and this lead to clay swelling phenomena, resulting in an enlarged interlayer space (e.g. Mooney et al., 1952a,b; Karaborni et al., 1996). Because of their high

* Corresponding author.
E-mail address: xiandongliu@gmail.com (X. Liu).

0016-7037/$ - see front matter © 2011 Elsevier Ltd. All rights reserved.
doi:10.1016/j.gca.2011.06.011

porosities and high specific surface areas, smectites not only play key roles in many natural processes but also find wide applications in engineering and industries (Bergaya et al., 2006). For example, people have utilized smectites for a long time in many fields such as environmental engineering, catalysis, and drug industry. Therefore, the naturally occurring 2-D nanopore architecture of smectites provides a good model system for studying the confinement effects for both theoretical and practical reasons. Indeed, people have been studying the novel properties of confined water and organics in clay interlayer spaces for decades. For example, according to numerous experimental and theoretical studies, it has been well recognized that in interlayer spaces, water can form integer-number molecular layers and organic ions (e.g. alkylammoniums) can form layering or paraffin configurations depending on the layer-charge characteristics (Mooney et al., 1952a,b; Bérend et al., 1995; Boek et al., 1995; Skipper et al., 1995a,b; Karaborni et al., 1996; Cases et al., 1997; Chang et al., 1998; Skipper, 1998; Smith, 1998; Sutton and Sposito, 2001; Tambach et al., 2004a,b; Lagaly et al., 2006; Liu and Lu, 2006; Skipper et al., 2006; Liu et al., 2007, 2008a, 2009; Cygan et al., 2009; Suter et al., 2009; Anderson et al., 2010).

Acidity is a fundamental aspect of molecular reactivity. Water molecules in interlayer space of clay minerals can donate protons and thus serve as the major Lewis acid sites in the interlayer regions (Bergaya et al., 2006). The 2-D environments alter the properties of confined waters from many aspects. (1) The hard clay layers physically limit the mobility of waters on the direction perpendicular to the basal surfaces. (2) The oxygen atoms on basal surfaces interact with interlayer waters via H-bonding. The clay layer charges polarize the waters to a large extent and thus impose effects on their interactions with surfaces. (3) Some counterions form strong chemical bonds with waters and thus rigid hydration shells. The positive charges of central cations repel protons of water ligands, which promote water dissociations. Furthermore, for the bound waters of cations close to solid surfaces, their p*K*as are also influenced by the surfaces, e.g. Criscenti and Sverjensky (1999). Based on these reasons, one can expect that the confined water has different acid–base properties from the bulk. Previous experimental studies (e.g. Mortland et al., 1963; Pinnavaia, 1983; Adams and McCabe, 2006) have indicated that some chemical reaction rates can be increased in smectites and from these observations, people have deduced that clay interlayer spaces enhance water acidity and that eventually accelerates the chemical reactions. However, since the chemical reactions occur in very narrow clay pores, it is still impossible to do *in situ* measurements of water acidity constants with modern experimental techniques. Therefore, up to now the absolute acidities of confined waters and the confinement effects of clay pores have not been revealed clearly. The lack of quantitative pictures not only makes it very difficult to uncover the acid–base chemistry of the interlayer waters but also prevents the further developments of practical applications (Adams and McCabe, 2006).

First principles molecular dynamics (FPMD) technique (Car and Parrinello, 1985), based on density functional theory and MD, has been proven a powerful tool to investigate proton transfer processes in condensed matters. The transfer of excess protons in liquid water has been studied with FPMD and the Grotthuss mechanisms are clearly illustrated (Tuckerman et al., 1997; Marx et al., 1999, 2010; Geissler et al., 2001; Tuckerman et al., 2002; Marx, 2006). By combining FPMD and free-energy calculation, Sprik (2000) investigated the self-dissociation of liquid water and predicted the p*K*w value to be about 13. Since that encouraging study, the methodology has been applied on more complicated condensed phase systems, e.g. pentaoxyphosphoranes (Davies et al., 2002; Doltsinis and Sprik, 2003), Al-aqua and $Si(OH)_4$ (Liu et al., 2010a), and carbonic acid conformers (Liu et al., 2010b). Recently, Churakov and Kosakowski (2010) employed FPMD to study the transfer events of excess protons occurring in the interlayer regions of smectites and found that similar to the bulk, the proton transfer processes are barrier free.

In this study, we employed FPMD technique to investigate the acid chemistry of the interlayer water molecules. The following points have been focused on: (1) the origin of promotion effects of clay interlayers, (2) the influences of layer charge densities and locations (i.e. tetrahedral and octahedral), and (3) the effects of counterion species. For these aims, both the charged and neutral clay pores are built for the purpose of comparisons. For the charged models, Na^+ and Mg^{2+}, the commonly occurring cations in clays, are taken as the interlayer counterions, which correspond to the low and high layer charge densities of clays, respectively. For Mg^{2+}-smectite models, the tetrahedral and octahedral substitutions are both considered. By using FPMD simulations, the interlayer microscopic structures of the models are characterized in detail. Then, the FPMD simulations combined with the method of constraint are carried out to investigate the dissociation mechanisms of the interlayer waters and thus, their acidity constants are derived. According to the detailed analyses, we theorize the clear picture about the effects of clay pores on acidities of water molecules.

2. METHODOLOGY

2.1. Systems

The clay framework model was derived from the report of Viani et al. (2002), which was also used in our previous simulations (Liu et al., 2008b; 2010a,b,c). The unit cell formula is $X^+_{(12\text{-}a\text{-}b)}[Si_aAl_{8\text{-}a}]\,[Al_bMg_{4\text{-}b}]O_{20}(OH)_4$, where X, $Al_{8\text{-}a}$and $Mg_{4\text{-}b}$ denote the monovalent counterion, isomorphic substitutions in tetrahedral and octahedral sheets, respectively. The crystallographic parameters are: $a = 5.18$ Å, $b = 8.98$ Å, $c = 10$ Å and $\alpha = \beta = \gamma = 90°$. The simulated systems (Fig. 1) consist of two unit cells ($2a \times b \times c$). For the neutral model, there is no isomorphic substitution in clay layers. For Na^+-smectite, one Mg replaces one Al in the octahedral sheet and a Na^+ ion is introduced into the interlayer region. For Mg^{2+}-smectites, two atoms are replaced in either the tetrahedral or the octahedral layer to give the framework a -2 charge and this charge is compensated by introducing one Mg^{2+} into the interlayer. For

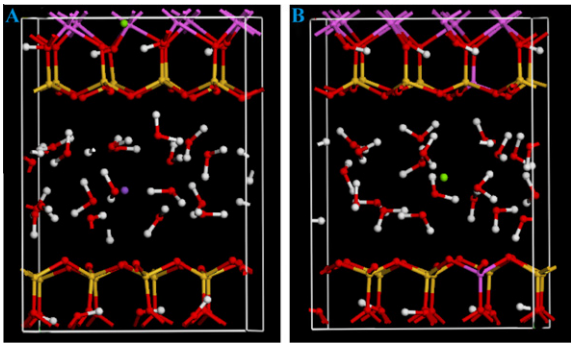

Fig. 1. Snapshots of (A) Na^{+}-smectite and (B) Mg^{2+}-smectite (tetrahedral substitution). In the pictures, Na = purple, O = red, H = white, Si = yellow, Al = light purple and Mg = green. (For interpretation of the references to colour in this figure legend, the reader is referred to the web version of this article.)

the tetrahedral one (named as Mg^{2+}-Tetra), two Al atoms replace two Si in the upper and the lower T-sheets, respectively and for the octahedral one (Mg^{2+}-Octa), two Mg atoms replace two Al which are not linked via an O.

Previous experimental and simulation studies have proved that Na^{+} and Mg^{2+} smectites can swell to 1 and 2 layer hydrates and in water rich environments, the 2-layer states are thermodynamically favorable over the 1-layer states (Brindley and Brown, 1980; Bérend et al., 1995; Cases et al., 1997; Whitley and Smith, 2004; Liu and Lu, 2006). Therefore, the models containing two water layers are focused on in this study. Based on our previous studies (Liu and Lu, 2006; Liu et al., 2008a), the 2-layer hydrate has about 10 water molecules per unit cell. With ($4a \times 2b \times 2c$) models, we carry out NPT MD simulations under ambient conditions to determine the basal spacing values. The simulations are performed by using LAMMPS package (Plimpton, 1995) and the CLAYFF force field (Cygan et al., 2004). The results show that for both Na^{+} and Mg^{2+} smectites models, the basal spacing values are around 15.0 Å. This value agrees well with previous experimental measurements (e.g. Brindley and Brown, 1980; Bérend et al., 1995; Cases et al., 1997). Therefore, the basal spacing and the final configurations are used to generate initial configurations for the following FPMD simulations.

For the systems of Na^{+} and Mg^{2+} in liquid water, the simulation cell is a periodically repeated cubic box of side length 10.5 Å. The cation-$(H_2O)_6$ complexes are placed at the center of the box and 32 water molecules are inserted around (about 1.4 mol/L), which approximately reproduces the density of water under ambient condition. For these charged systems, neutralizing background charges are added in the simulations (Marx and Hutter, 2009).

2.2. Car–Parrinello MD

The electronic structures are calculated by using density functional theory with the BLYP functional (Becke, 1988; Lee et al., 1988), which can accurately describe the behaviors of water and proton (e.g. Laasonen et al., 1993; Sprik et al., 1996; Marx et al., 1999, 2010; Marx, 2006). The norm-conserving Martins–Trouillier pseudopotentials (Troullier and Martins, 1991) with the Kleinman-Bylander scheme (Kleinman and Bylander, 1982) are used to describe the interactions of the valence electrons and the core states. The orbitals are expanded in plane wave basis sets with a kinetic energy cutoff of 70 Ry.

All FPMD simulations are performed with the CPMD package (CPMD version 3.11.2) (Car and Parrinello, 1985). All hydrogen atoms are assigned a mass of deuterium. The fictitious electronic mass is set to 800 a.u. and the equation of motion is integrated with a time step of 0.144 fs, which maintains the adiabatic conditions of CPMD. The temperature is controlled at 300 K with the Nosé-Hoover chain thermostat. For the constrained simulation, MD is carried out with the reaction coordinate fixed at the desired value. Each unconstrained/constrained MD trajectory includes a production step of 12 ps and a prior equilibration run of at least 3 ps. The statistics are collected every six steps for all simulations.

2.3. p*K*a calculation and method of constraint

For the dissociation reaction of liquid water $H_2O \rightarrow H^{+} + OH^{-}$ with a free energy change ΔF, the acidity of the water can be calculated with,

$$\mathrm{p}Ka = \frac{\Delta F}{k_B T \ln(10)} \tag{1}$$

Here k_B and T are Boltzmann constant and temperature, respectively.

The dissociation reaction event is enforced to happen with the method of constraint and the relative free energies (ΔF) are calculated by integrating the averaged force (f) along the reaction coordinates via the thermodynamic integration relation (Carter et al., 1989; Sprik and Ciccotti, 1998),

$$\Delta F(\mathrm{Q}) = -\int_{Q_0}^{Q} dQ' f(Q') \tag{2}$$

Here the coordination number (CN) of the reactive hydroxyl oxygen is selected as the reaction coordinate (Q) to represent the reaction progress.

In the simulations, the CN of the reactive oxygen (O^{*}) runs over all water hydrogen in the model,

$$n_H = \sum_{i=1}^{N_H} S(|r_{H_i} - r_{O*}|) \tag{3}$$

The function $S(r)$ is used to weight the contributions of all water hydrogen with a suitable distance dependent function. In this study we employ the Fermi function (Sprik, 1998, 2000),

$$S(r) = \frac{1}{\exp[\kappa(r - r_c)] + 1} \tag{4}$$

where κ and r_c denote the inversion of the width and the cutoff and the hydrogen atoms outside the interval of $r_c - \kappa < r < r_c + \kappa$ are effectively counted as 1 or 0. In our calculations, 0.10 Å and 1.35 Å are used for κ and r_c, respectively.

As mentioned above, all hydrogen has a mass of D for computation efficiency. Because the nuclei are treated as classical particles in the used CPMD technique, the quantum effects of hydrogen cannot be captured. Therefore, the subtle acidity differences of D and H (pK_w (D_2O) − pK_W(H_2O) ≈ 0.7 (Wynne-Jones, 1936)) would not be distinguished. For the purpose of clarity, we use H_2O instead of D_2O in the text.

Within constrained FPMD simulation times (~15 ps), the mean forces can reach reasonable convergences within 1.8 kcal/mol. (see the electronic annex). This sets an upper limit of 1.1 p*K*a units to the statistical uncertainty in our acidity calculations.

3. RESULTS AND DISCUSSIONS

3.1. Interlayer structures

The density profiles of interlayer atomic species are derived to characterize the interlayer structures (Fig. 2). On these plots, the middle planes of the pores are taken as the origins and the distances (−4 to 4 Å) approximately correspond to the distances between the basal oxygen planes above and below the origins because the pore widths are around 8 Å. All density curves of water oxygen show two well separated peaks, which indicates the water molecules form two layers. On all plots, the density curves of water hydrogen represent considerable distributions in the middle, indicating that some H-bonds exist between the lower and upper water layers. For the neutral pore, the hydrogen mainly distributes from −2.5 to 2.5 Å on the distance axis, i.e. they are mostly over 1.5 Å away from the clay surfaces. In contrast, for the three charged models, hydrogen represents considerable distributions in the ranges <1.5 Å away from the surfaces. This obvious difference is caused by the layer charges, which encourages H-bonding between water hydrogen and surface oxygen atoms.

For Na^+-smectite, the cation shows a distribution peaked at about 1.0 Å (Fig. 2B), indicating that Na^+ cations do not favor staying around the midplane. As revealed by the radial distribution function curve of cation-water oxygen (Fig. 3A), the first peak ranges from 2.0 to 3.0 Å, which amounts to about five on the accumulated coordination number profile. Fig. 4A illustrates a representative snapshot, which shows that Na^+ binds to one basal oxygen and five water molecules. This observation is consistent with a previous CPMD simulation report (Suter et al., 2008). In that study, they found that the most stable complex has a very similar configuration as shown in Fig. 4A, which is of a lower free-energy than that one located at the exact midplane.

For both Mg^{2+}-smectites, the cations reside around the midplanes during the simulations (Fig. 2C and D). Mg^{2+}-O RDF curves (Fig. 3B and C) show very sharp first peaks ranging 1.9–2.5 Å and the accumulated coordination number curves indicate that Mg^{2+} cations form very structured first hydration shells consisting of six waters (Callahan et al., 2010). This is consistent with the previous classical MD study of Mg^{2+} cations in clay interlayers (Greathouse et al., 2000). The derived snapshot (Fig. 4B) illustrates the octahedral hydration shell.

In the simulation of Na^+-smectite, it is found that the hydration shell of Na^+ is very flexible and the exchange between the 1st shell and the other waters happens quite frequently. Fig. 5 plots the trajectories of distances between the cations and the leaving waters for in liquid water and in smectite interlayer. One can see that for both cases the first shell waters leave on a picosecond timescale, which

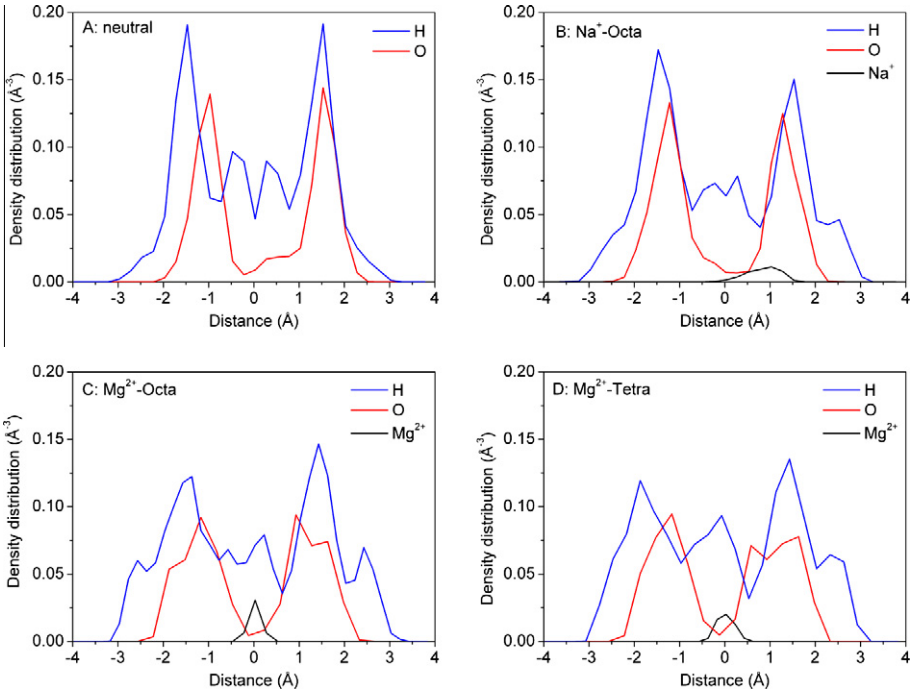

Fig. 2. Density distributions of interlayer species.

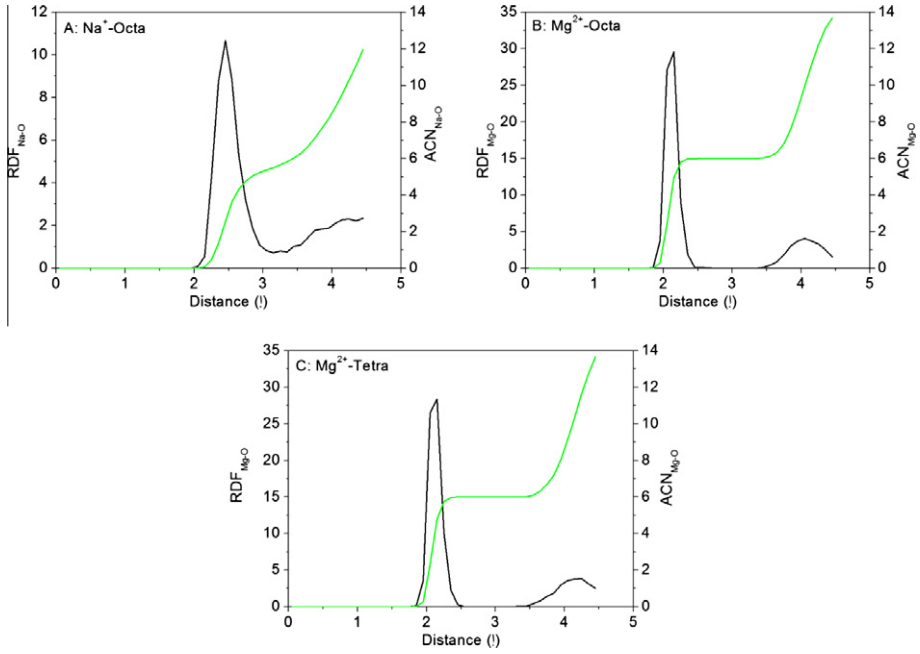

Fig. 3. RDFs (radial distribution functions) and ACNs (accumulated coordination numbers) of water oxygen around metal cations in the interlayer spaces.

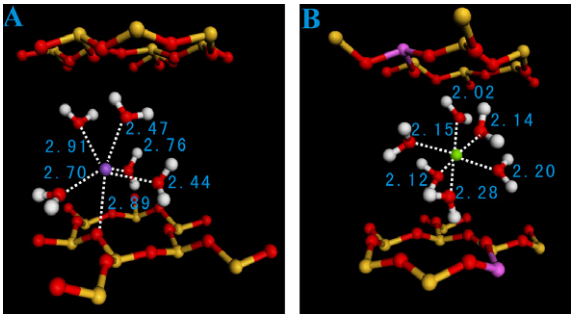

Fig. 4. Coordination structures of counterions in (A) Na^{+}-smectite and (B) Mg^{2+}-smectite (tetrahedral substitution). For the purpose of clarity, the other water molecules are removed. In the pictures, Na = purple, O = red, H = white, Si = yellow, Al = light purple and Mg = green. (For interpretation of the references to colour in this figure legend, the reader is referred to the web version of this article.)

indicates that the interaction between Na^{+} and water is relatively weak. In contrast, the hydration shell of Mg^{2+} is very rigid and no exchange event has been observed during the simulations.

3.2. Acid chemistry

3.2.1. pKas of Na^{+}-aqua and Mg^{2+}-aqua in liquid water

As shown in Fig. 6, the calculated free energy change for the dissociation of a water molecule bound to Mg^{2+} in liquid water is about 16 kcal/mol and the p*K*a is about 11.8. This result coincides well with the experimental measurement, 11.4 (Westermann et al., 1986). In a previous AIMD study of Mg^{2+} (Bernasconi et al., 2006), 11.6 was obtained with a slightly different post-processing approach. For Na^{+} in water, due to the water exchange as discussed above, the focused water molecule would quickly get off from the first shell in the simulation and therefore, the final

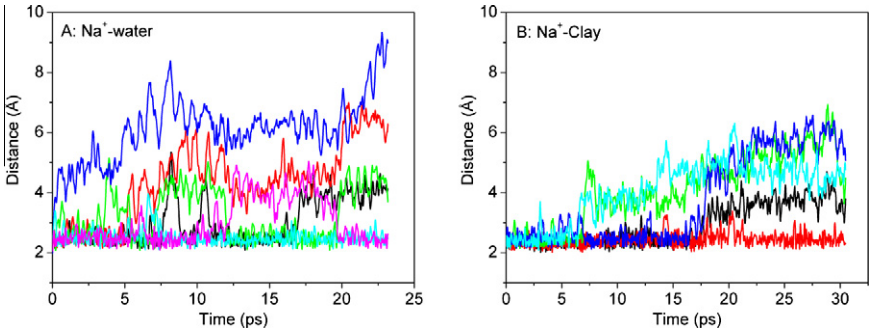

Fig. 5. The trajectories of distances between Na^{+} and the leaving water molecules in the simulations: (A) Na^{+} in liquid water and (B) Na^{+} in interlayer space of smectite.

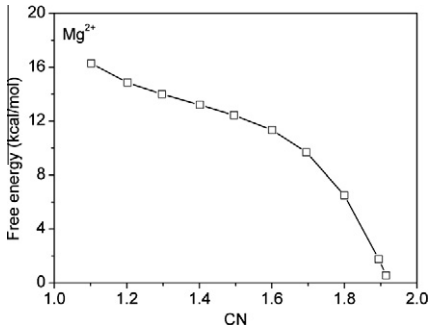

Fig. 6. Free energy profile for the dissociation of a 1st-shell water of Mg^{2+} as a function of the number of H around the reactive O (CN). The curve is used to guide eyes.

result is actually equal to the p*K*w, 13.0 (Sprik, 2000). This also explains why Na^{+} hardly influences the dissociations of water molecules (Westermann et al., 1986).

3.2.2. General pictures of confined water dissociation

For the neutral model and Na^{+}-smectite, all waters are equal and thus the dissociating water molecules are selected randomly. For the two Mg^{2+}-smectites, one bound water (i.e. one in $Mg(H_2O)_6^{2+}$) and one free water are selected to do the dissociation simulations, respectively.

To show the water dissociating process, the simulations of bound water in Mg^{2+}-Octa are taken as an illustrative example (Fig. 7). On the initial steps (CN = 1.8, Fig. 7A), the breaking O–H bond is stretched a little from the equilibrium and the H-bond between the leaving proton and the

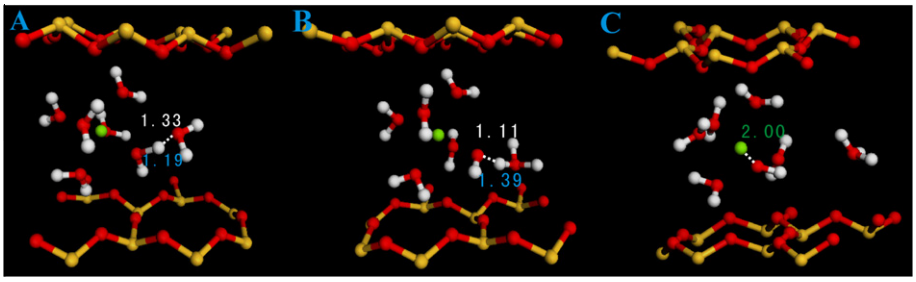

Fig. 7. Snapshots derived from the dissociation simulations of 1st-shell water in Mg^{2+}-smectite (octahedral substitution). For the purpose of clarity, the other water molecules are removed. (A) CN = 1.8, (B) CN = 1.5, and (C) CN = 1.2. In the pictures, O = red, H = white, Si = yellow, Al = light purple and Mg = green. The white numbers denote the bonds between the leaving proton and the accepting oxygen, the blue numbers indicate the bonds between the leaving proton and the donating oxygen. (For interpretation of the references to colour in this figure legend, the reader is referred to the web version of this article.)

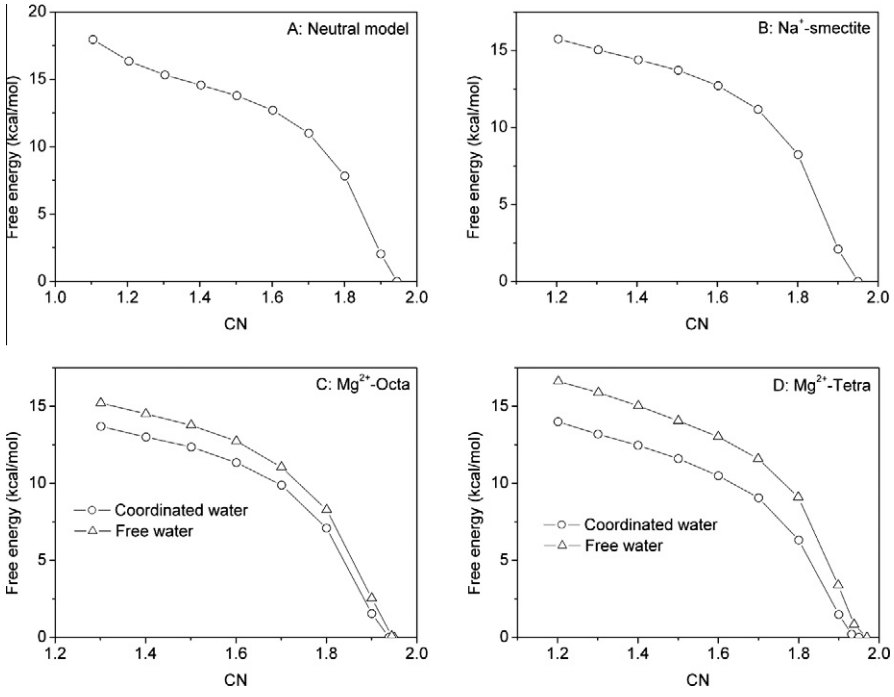

Fig. 8. Free energy profiles calculated for water dissociations in clay interlayer spaces. The curves are used to guide eyes.

Table 1
Calculated p*K*a values of confined waters. The values for bulk water, Na^+-aqua, and Mg^{2+}-aqua are included for comparison.

System		p*K*a
Bulk water/Na^+		13.0
Mg^{2+}		11.8
Neutral model		12.6
Na^+-smectite		11.5
Mg^{2+}-Octa	Bound water	10.1
	Free water	11.3
Mg^{2+}-Tetra	Bound water	10.4
	Free water	12.1

acceptor water would become stronger. As the CN decreases to 1.5, the leaving proton binds to the acceptor water and the hydronium ion has formed (Fig. 7B). At CN = 1.2, the Grotthuss mechanism is initiated (Marx, 2006) and the proton freely diffuses to other water molecules (Fig. 7C). It can be seen that after hydrolysis, Mg^{2+}–O bond length decreases to around 2.0 Å from the initial 2.12 Å (Fig. 7C).

The integrated free-energy curves are shown in Fig. 8 and the calculated p*K*a values are collected in Table 1.

3.2.3. pKas of confined waters

The calculated p*K*a in the neutral pore is around 12.6. This is quite close to the BLYP result of the liquid water, 13.0 (Sprik, 2000). In contrast, for all the other interlayer waters, the p*K*a values are obviously smaller than the bulk value. This clearly reveals that the enhancement of water dissociation mainly stems from the layer charges whereas the geometrical constraint effect is trivial.

The p*K*a value of the water in Na^+-smectite is 11.5. That is near the acidity of the free water in the octahedrally-substituted Mg^{2+}-smectite, 11.3. Such acidity should be considered significant, since they are close to the p*K*a of Mg^{2+}-aqua and Mg^{2+} has proven an active role of acidic catalyst in many (bio)chemical reactions (Cowan, 1995; Sigel and Pyle, 2007). Furthermore, it can be deduced that increasing the layer charge density from 0.5 *e* to 1.0 *e* does not cause obvious effect on the acidity of free waters. 1 *e* per unit cell is almost the upper limit of smectites (Bergaya et al., 2006) and therefore, the value derived here (i.e. 11.3) can be considered to be the lower limit of free waters' acidity in clay pores.

The waters coordinated by Mg^{2+} in both smectites represent significantly low p*K*a values, 10.1 and 10.4. Therefore, one can see that for both Mg^{2+}-smectites, the p*K*as of coordinated and free waters agree with their respective counterpart values within 1 p*K*a unit. This strongly suggests that substitution positions do not lead to obvious differences. By comparing the values of coordinated waters with the p*K*a of Mg^{2+}-aqua in the bulk, it can be concluded that clay layers can obviously promote the dissociation of bound waters.

Like Mg^{2+}, other divalent cations such as Ca^{2+}, Sr^{2+} have very high hydration energies (over 1000 kJ/mol) and in interlayer regions of smectites they also prefer forming outer-sphere complexes (e.g. Chávez-Páez et al., 2001; Whitley and Smith, 2004). Therefore, the findings derived for Mg^{2+} also hold true for those cations. Given that more acidic trivalent cations (e.g. Al^{3+}, Fe^{3+}) are present in interlayers, their acidities can also be enhanced by clay frameworks. That would make the interlayer region a much more acidic environment than the bulk and therefore, many geochemical/biochemical processes can be catalyzed there.

4. CONCLUSIONS

In this study, the acid chemistry of confined waters in interlayer space of smectites is investigated with FPMD simulations. The method of constraint is employed to enforce the reactions and thermodynamic integration is used to derive the free-energy changes and thus the acidity constants. Three possible controlling factors have been taken into account: layer charge densities (0 *e*, 0.5 *e* and 1.0 *e* per unit cell), layer charge locations (tetrahedral vs octahedral) and interlayer counterions (Na^+ vs Mg^{2+}). According to detailed analyses, the following points have been achieved.

(1) Na^+ and Mg^{2+} cations show significantly different complexing characteristics in clay pores. Mg^{2+} forms a very rigid octahedral hydration shell and behaves as outer-sphere complexes. Na^+ binds to one basal oxygen atom and forms a very flexible hydration shell of five waters on average, which shows very fast water exchanges. This explains why Mg^{2+} promotes water dissociation obviously but Na^+ almost does not.
(2) The neutral clay framework does not enhance water dissociations whereas all charged do. This evidences that layer charge is the direct origin for enhancing the acidity of interlayer water.
(3) With a moderate charge density 0.5 *e* per unit cell, the interlayer water shows a p*K*a of 11.5 in smectites. Increasing layer charge density to 1.0 *e* does not lead to obvious further enhancement on the acidities of the free water molecules. Because 1.0 *e* is at the upper limit of charge densities of smectites, we propose that the acidity calculated here (11.3) can be viewed as the lower limit of the acidities of free interlayer waters.
(4) The 1st-shell waters of Mg^{2+} show very low p*K*a values (10.1 vs 10.4) for octahedrally and tetrahedrally substituted models. By comparing them with the bulk value of Mg^{2+}-aqua, 11.8, it is clear that clay frameworks can also enhance acidities of the cation-bound waters. Because many highly acidic cations (e.g. Mg^{2+}, Ca^{2+}, Al^{3+}, Fe^{3+}) occur as counterions in nature, their presence eventually makes the interlayer region a chemical environment of high acid activity. Furthermore, the results of the two Mg^{2+}-models reveals that layer charge locations show trivial influences on the acidities of both free and coordinated waters.

ACKNOWLEDGMENTS

We thank Dr. Donald Sparks, Dr. Frank Podosek and anonymous reviewers for their generous helps on improving the paper.

We are grateful to the High Performance Computing Center of Nanjing University for doing the calculations on its IBM Blade cluster system. Authors acknowledge Natural Science Foundation of China (Nos. 41002013 and 40973029), Natural Science Foundation of Jiangsu Province (BK2010008), and the support (No. 2009-II-3) from the State Key Laboratory for Mineral Deposits Research, Nanjing University.

APPENDIX A. SUPPLEMENTARY DATA

Supplementary data associated with this article can be found, in the online version, at doi:10.1016/j.gca.2011.06.011.

REFERENCES

Adams J. M. and McCabe R. W. (2006) Clay minerals as catalysts. In *Handbook of Clay Science* (eds. F. Bergaya, B. G. K. Theng and G. Lagaly). Elsevier, Amsterdam, pp. 541–582.

Anderson R. L., Ratcliffe I., Greenwell H. C., Williams P. A., Cliffe S. and Coveney P. V. (2010) Clay swelling – A challenge in the oilfield. *Earth-Sci. Rev.* **98**, 201–216.

Becke A. D. (1988) Density-functional exchange-energy approximation with correct asymptotic-behavior. *Phys. Rev. A* **38**, 3098–3100.

Bérend I., Cases J. M., François M., Uriot J. P., Michot L., Masion A. and Thomas F. (1995) Mechanism of adsorption and desorption of water vapor by homoionic montmorillonites: 2. The Li^+, Na^+, K^+, Rb^+ and Cs^+-exchanged forms. *Clays Clay Miner.* **43**, 324–336.

Bergaya F., Theng B. G. K. and Lagaly G. (2006) *Handbook of Clay Science*. Elsevier, Amsterdam.

Bernasconi L., Baerends E. J. and Sprik M. (2006) Long-range solvent effects on the orbital interaction mechanism of water acidity enhancement in metal ion solutions: a comparative study of the electronic structure of aqueous Mg and Zn dications. *J. Phys. Chem. B* **110**, 11444–11453.

Bleam W. F. (1993) Atomic theories of phyllosilicates: Quantum chemistry, statistical mechanics, electrostatic theory, and crystal chemistry. *Reviews of Geophysics* **31**, 51–73.

Boek E. S., Coveney P. V. and Skipper N. T. (1995) Monte Carlo molecular modeling studies of hydrated Li-, Na-, and K-smectites: understanding the role of potassium as a clay swelling inhibitor. *J. Am. Chem. Soc.* **117**, 12608–12617.

Brindley G. W. and Brown G. (1980) *Crystal Structures of Clay Minerals and their X-ray Identification*. Mineralogical Society, London.

Callahan K. M., Casillas-Ituarte N. N., Roeselova M., Allen H. C. and Tobias D. J. (2010) Solvation of magnesium dictation: molecular dynamics simulation and vibrational spectroscopic study of magnesium chloride in aqueous solutions. *J. Phys. Chem. A* **114**, 5141–5148.

Car R. and Parrinello M. (1985) Unified approach for molecular-dynamics and density-functional theory. *Phys. Rev. Lett.* **55**, 2471–2474.

Carter E. A., Ciccotti G., Hynes J. T. and Kapral R. (1989) Constrained reaction coordinate dynamics for the simulation of rare events. *Chem. Phys. Lett.* **156**, 472–477.

Cases J. M., Berend I., Francois M., Uriot J. P., Michot L. J. and Thomas F. (1997) Mechanism of adsorption and desorption of water vapor by homoionic montmorillonite: 3. The Mg^{2+}, Ca^{2+}, Sr^{2+} and Ba^{2+} exchanged forms. *Clays Clay Miner.* **45**, 8–22.

Chang F.-R. C., Skipper N. T. and Sposito G. (1998) Monte Carlo and molecular dynamics simulations of electrical double-layer structure in potassium-montmorillonite hydrates. *Langmuir* **14**, 1201–1207.

Chávez-Páez M., van Workum K., de Pablo L. and de Pablo J. J. (2001) Monte Carlo simulations of Ca-montmorillonite hydrates. *J. Chem. Phys.* **114**, 1405–1413.

Churakov S. V. and Kosakowski G. (2010) An ab initio molecular dynamics study of hydronium complexation in Na-montmorillonite. *Phil. Mag.* **90**, 2459–2474.

Cowan J. A. (1995) *Biological Chemistry of Magnesium*. VCH, New York.

Criscenti L. J. and Sverjensky D. A. (1999) The role of electrolyte anions (ClO_4^-, NO_3^-, and Cl^-) in divalent metal (M^{2+}) adsorption on oxide and hydroxide surfaces in salt solutions. *Am. J. Sci.* **299**, 828–899.

Cygan R. T., Greathouse J. A., Heinz H. and Kalinichev A. G. (2009) Molecular models and simulations of layered materials. *J. Mater. Chem.* **19**, 2470–2481.

Cygan R. T., Liang J. J. and Kalinichev A. G. (2004) Molecular models of hydroxide, oxyhydroxide, and clay phases and the development of a general force field. *J. Phys. Chem. B* **108**, 1255–1266.

Davies J. E., Doltsinis N. L., Kirby A. J., Roussev C. D. and Sprik M. (2002) Estimating p*K*(a) values for pentaoxyphosphoranes. *J. Am. Chem. Soc.* **124**, 6594–6599.

Doltsinis N. L. and Sprik M. (2003) Theoretical p*K*(a) estimates for solvated P(OH)(5) from coordination constrained Car–Parrinello molecular dynamics. *Phys. Chem. Chem. Phys.* **5**, 2612–2618.

Dysthe D. K. and Wogelius R. A. (2006) Physics and chemistry of confined fluids. *Chem. Geol.* **230**, 175–242.

Geissler P. L., Dellago C., Chandler D., Hutter J. and Parrinello M. (2001) Autoionization in liquid water. *Science* **291**, 2121–2124.

Greathouse J. A., Refson K. and Sposito G. (2000) Molecular dynamics simulation of water mobility in magnesium-smectite hydrates. *J. Am. Chem. Soc.* **122**, 11459–11464.

Grim R. E. (1962) *Applied Clay Mineralogy*. McGraw-Hill, New York.

Karaborni S., Smit B., Heidug W., Urai J. and Van Oort E. (1996) The swelling of clays: molecular simulations of the hydration of montmorillonite. *Science* **271**, 1102–1104.

Kleinman L. and Bylander D. M. (1982) Efficacious form for model pseudopotentials. *Phys. Rev. Lett.* **48**, 1425–1428.

Laasonen K., Sprik M., Parrinello M. and Car R. (1993) Ab-initio liquid water. *J. Chem. Phys.* **99**, 9080–9089.

Lagaly G., Ogawa M. and Dekany I. (2006) Clay mineral organic interactions. In *Handbook of Clay Science* (eds. F. Bergaya, B. G. K. Theng and G. Lagaly). Elsevier, Amsterdam, pp. 309–377.

Lee C., Yang W. and Parr R. G. (1988) Development of the colle-salvetti correlation-energy formula into a functional of the electron-density. *Phys. Rev. B* **37**, 785–789.

Liu X. D. and Lu X. C. (2006) A thermodynamic understanding of clay-swelling inhibition by potassium ions. *Angew. Chem. Int. Edit.* **45**, 6300–6303.

Liu X. D., Lu X. C., Meijer E. J., Wang R. C. and Zhou H. Q. (2010a) Acid dissociation mechanisms of Si(OH)(4) and $Al(H_2O)(6)(3^+)$ in aqueous solution. *Geochim. Cosmochim. Acta* **74**, 510–516.

Liu X. D., Lu X. C., Wang R. C. and Zhou H. Q. (2008a) Effects of layer charge distribution on the thermodynamic and microscopic properties of Cs-smectite. *Geochim. Cosmochim. Acta* **72**, 1837–1847.

Liu X. D., Lu X. C., Wang R. C. and Zhou H. Q. (2010b) In silico calculation of acidity constants of carbonic acid conformers. *J. Phys. Chem. A* **114**, 12914–12917.

Liu X. D., Lu X. C., Wang R. C., Zhou H. Q. and Xu S. J. (2007) Interlayer structures and dynamics of alkylammonium-intercalated smectites with and without water: a molecular dynamic study. *Clays Clay Miner.* **55**, 554–564.

Liu X. D., Lu X. C., Wang R. C., Zhou H. Q. and Xu S. J. (2008b) Surface complexes of acetate on edge surfaces of 2:1 type phyllosilicate: insights from density functional theory calculation. *Geochim. Cosmochim. Acta* **72**, 5896–5907.

Liu X. D., Lu X. C., Wang R. C., Zhou H. Q. and Xu S. J. (2009) Molecular dynamics insight into the cointercalation of HDTMA and acetate ions into smectites. *Am. Mineral.* **94**, 143–150.

Liu X. D., Meijer E. J., Lu X. C. and Wang R. C. (2010c) Ab initio molecular dynamics study of iron-containing smectites. *Clays Clay Miner.* **58**, 89–96.

Marx D. (2006) Proton transfer 200 years after von Grotthuss: insights from ab initio simulations. *ChemPhysChem* **7**, 1848–1870.

Marx D., Chandra A. and Tuckerman M. E. (2010) Aqueous basic solutions: hydroxide solvation, structural diffusion, and comparison to the hydrated proton. *Chem. Rev.* **110**, 2174–2216.

Marx D., Tuckerman M. E., Hutter J. and Parrinello M. (1999) The nature of the hydrated excess proton in water. *Nature* **397**, 601–604.

Marx D. and Hutter J. (2009) *Ab Initio Molecular Dynamics – Basic Theory and Advanced Methods*. Cambridge University Press, Cambridge.

Mooney R. W., Keenan A. G. and Wood L. A. (1952a) Adsorption of water vapor by montmorillonite. I. Heat of desorption and application of BET Theory. *J. Am. Chem. Soc.* **74**, 1367–1371.

Mooney R. W., Keenan A. G. and Wood L. A. (1952b) Adsorption of water vapor by montmorillonite. II. Effect of exchangeable ions and lattice swelling as measured by X-ray diffraction. *J. Am. Chem. Soc.* **74**, 1371–1374.

Mortland M. M., Fripiat J. J., Chaussidon J. and Uytterhoeven J. B. (1963) Interaction between ammonia and the expanding lattices of montmorillonite and vermiculite. *J. Phys. Chem.* **67**, 248–258.

Pinnavaia T. J. (1983) Intercalated clay catalysts. *Science* **220**, 365–371.

Plimpton S. J. (1995) Fast parallel algorithms for short-range molecular dynamics. *J. Comput. Phys.* **117**, 1–19.

Brovchenko I. and Oleinikova A. (2008) *Interfacial and Confined Water*. Elsevier Science, Amsterdam.

Sigel R. K. O. and Pyle A. M. (2007) Alternative roles for metal ions in enzyme catalysis and the implications for ribozyme chemistry. *Chem. Rev.* **107**, 97–113.

Skipper N. T. (1998) Computer simulation of aqueous pore fluids in 2:1 clay minerals. *Mineral. Mag.* **62**, 657–667.

Skipper N. T., Chang F.-R. C. and Sposito G. (1995a) Monte Carlo simulation of interlayer molecular structure in swelling clay minerals. 1. Methodology. *Clays Clay Miner.* **43**, 294–303.

Skipper N. T., Chang F.-R. C. and Sposito G. (1995b) Monte Carlo simulation of interlayer molecular structure in swelling clay minerals. 2. Monolayer hydrates. *Clays Clay Miner.* **43**, 294–303.

Skipper N. T., Lock P. A., Titiloye J. O., Swenson J., Mirza Z. A., Howells W. S. and Fernandez-Alonso F. (2006) The structure and dynamics of 2-dimensional fluids in swelling clays. *Chem. Geol.* **230**, 182–196.

Smith D. E. (1998) Molecular computer simulations of the swelling properties and interlayer structure of cesium montmorillonite. *Langmuir* **14**, 5959–5967.

Sprik M. (1998) Coordination numbers as reaction coordinates in constrained molecular dynamics. *Faraday Discuss.* **110**, 437–445.

Sprik M. (2000) Computation of the pK of liquid water using coordination constraints. *Chem. Phys.* **258**, 139–150.

Sprik M. and Ciccotti G. (1998) Free energy from constrained molecular dynamics. *J. Chem. Phys.* **109**, 7737–7744.

Sprik M., Hutter J. and Parrinello M. (1996) Ab initio molecular dynamics simulation of liquid water: comparison three gradient-corrected density functionals. *J. Chem. Phys.* **105**, 1142–1152.

Suter J. L., Anderson R. L., Greenwell H. C. and Coveney P. V. (2009) Recent advances in large-scale atomistic and coarse-grained molecular dynamics simulation of clay minerals. *J. Mater. Chem.* **19**, 2482–2493.

Suter J. L., Boek E. S. and Sprik M. (2008) Adsorption of a sodium ion on a smectite clay from constrained ab initio molecular dynamics simulations. *J. Phys. Chem. C* **112**, 18832–18839.

Sutton R. and Sposito G. (2001) Molecular simulation of interlayer structure and dynamics in 12.4 Å Cs-smectite hydrates. *J. Colloid Interf. Sci.* **237**, 174–184.

Tambach T. J., Hensen E. J. M. and Smit B. J. (2004a) Molecular simulations of swelling clay minerals. *J. Phys. Chem. B* **108**, 7586–7596.

Tambach T. J., Bolhuis P. G. and Smit B. (2004b) A molecular mechanism of hysteresis in clay swelling. *Angew. Chem. Int. Edit.* **43**, 2650–2652.

Troullier N. and Martins J. L. (1991) Efficient pseudopotentials for plane-wave calculations. *Phys. Rev. B* **43**, 1993–2006.

Tuckerman M. E., Marx D. and Parrinello M. (2002) The nature and transport mechanism of hydrated hydroxide ions in aqueous solution. *Nature* **417**, 925–929.

Tuckerman M. E., Marx D., Klein M. L. and Parrinello M. (1997) On the quantum nature of the shared proton in hydrogen bonds. *Science* **275**, 817–820.

Viani A., Gaultieri A. F. and Artioli G. (2002) The nature of disorder in montmorillonite by simulation of X-ray powder patterns. *Am. Mineral.* **87**, 966–975.

Wang Y. F., Bryan C., Xu H. F. and Gao H. Z. (2003) Nanogeochemistry: geochemical reactions and mass transfers in nanopores. *Geology* **31**, 387–390.

Westermann K., Naser K.-H. and Brandes G. (1986) *Inorganic Chemistry (Anorganische Chemie), 12th ed.*. VEB Deutscher Verlag fiir Grundstoffindustrie, Leipzig, GDR.

Whitley H. D. and Smith D. E. (2004) Free energy, energy, and entropy of swelling in Cs-, Na-, and Sr-montmorillonite clays. *J. Chem. Phys.* **120**, 5387–5395.

Wynne-Jones W. F. K. (1936) The electrolytic dissociation of heavy water. *Trans. Faraday Soc.* **32**, 1397–1402.

Associate editor: Donald L. Sparks